The diabetes-susceptible gene *SLC30A8*/ZnT8 regulates hepatic insulin clearance

Motoyuki Tamaki,[1] Yoshio Fujitani,[1,2,3] Akemi Hara,[2] Toyoyoshi Uchida,[1] Yoshifumi Tamura,[1,4] Kageumi Takeno,[1] Minako Kawaguchi,[1] Takahiro Watanabe,[1] Takeshi Ogihara,[1] Ayako Fukunaka,[1,2] Tomoaki Shimizu,[1] Tomoya Mita,[1,5] Akio Kanazawa,[1,6] Mica O. Imaizumi,[7] Takaya Abe,[8] Hiroshi Kiyonari,[8] Shintaro Hojyo,[9] Toshiyuki Fukada,[9,10] Takeshi Kawauchi,[11,12] Shinya Nagamatsu,[7] Toshio Hirano,[9,13] Ryuzo Kawamori,[1,4] and Hirotaka Watada[1,2,4,5,6]

[1]Department of Metabolism and Endocrinology, [2]Center for Beta-Cell Biology and Regeneration, [3]JST-CREST Program, [4]Sportology Center, [5]Center for Molecular Diabetology, and [6]Center for Therapeutic Innovations in Diabetes, Juntendo University Graduate School of Medicine, Tokyo, Japan. [7]Department of Biochemistry, Kyorin University School of Medicine, Tokyo, Japan. [8]Laboratories for Animal Resources and Genetic Engineering, RIKEN Center for Developmental Biology, Kobe, Japan. [9]Laboratory of Cytokine Signaling, RIKEN Research Center for Allergy and Immunology, Yokohama, Japan. [10]Department of Allergy and Immunology, Graduate School of Medicine, Osaka University, Osaka, Japan. [11]Precursor Research for Embryonic Science and Technology (PRESTO), Japan Science and Technology Agency (JST), Saitama, Japan. [12]Department of Physiology, Keio University School of Medicine, Tokyo, Japan. [13]JST-CREST Program, Osaka University, Osaka, Japan.

Recent genome-wide association studies demonstrated that common variants of solute carrier family 30 member 8 gene (*SLC30A8*) increase susceptibility to type 2 diabetes. *SLC30A8* encodes zinc transporter-8 (ZnT8), which delivers zinc ion from the cytoplasm into insulin granules. Although it is well known that insulin granules contain high amounts of zinc, the physiological role of secreted zinc remains elusive. In this study, we generated mice with β cell–specific *Slc30a8* deficiency (ZnT8KO mice) and demonstrated an unexpected functional linkage between *Slc30a8* deletion and hepatic insulin clearance. The ZnT8KO mice had low peripheral blood insulin levels, despite insulin hypersecretion from pancreatic β cells. We also demonstrated that a substantial amount of the hypersecreted insulin was degraded during its first passage through the liver. Consistent with these findings, ZnT8KO mice and human individuals carrying rs13266634, a major risk allele of *SLC30A8*, exhibited increased insulin clearance, as assessed by c-peptide/insulin ratio. Furthermore, we demonstrated that zinc secreted in concert with insulin suppressed hepatic insulin clearance by inhibiting clathrin-dependent insulin endocytosis. Our results indicate that *SLC30A8* regulates hepatic insulin clearance and that genetic dysregulation of this system may play a role in the pathogenesis of type 2 diabetes.

Introduction

Recent genome-wide association studies demonstrated that individuals with the R325W polymorphism of solute carrier family 30 member 8 gene (*SLC30A8*), rs13266634, are at high risk for type 2 diabetes (1–5). *SLC30A8* encodes zinc transporter-8 (ZnT8), which delivers zinc ion from the cytoplasm of pancreatic β cells to insulin granules (6). Insulin granules contain high amounts of zinc, and zinc that is cosecreted with insulin affects neighboring endocrine cells in the islets of Langerhans in both paracrine and autocrine fashions (7–11). While studies of ZnT8 deletion or overexpression in insulinoma cells have suggested that it contributes to the maintenance of glucose-stimulated insulin secretion (GSIS) (12, 13), others have reported that zinc suppresses insulin secretion from pancreatic β cells (8–10, 14–16). In addition, recent loss-of-function studies of *Slc30a8* in mice demonstrated that ZnT8 is important for the crystallization of insulin molecules and efficient insulin processing in insulin granules, but there is no agreement on the precise role of ZnT8 in increased susceptibility to type 2 diabetes (17–21). In the EUGENE2 study, human homozygous carriers of the C risk allele of *SLC30A8* showed lower peripheral insulin levels in the early phase of i.v. glucose tolerance test (GTT) (22), which suggests that *SLC30A8* might regulate insulin homeostasis.

Insulin secreted from the islets of Langerhans flows directly into the portal vein (PV). About half of the insulin that enters the liver is cleared, while the rest flows into the systemic circulation (23). Thus, the rate of hepatic insulin clearance is an important regulator of peripheral insulin level. In the postprandial state, hepatic insulin clearance is estimated to be suppressed by 20% (24). Although incretin hormones, such as glucagon-like peptide–1 (GLP-1) and gastric inhibitory polypeptide (GIP), which are secreted with food intake, have been proposed to be regulators of hepatic insulin clearance (25, 26), a later study argued against this possibility (27). Another report implicated the insulin pulse mass from pulsatile insulin secretion into the PV in suppressing hepatic insulin clearance rate (28, 29), but the mechanism underlying this process was not fully elucidated.

In the present study, we provide evidence that zinc is cosecreted with insulin in a ZnT8-dependent manner, and that the secreted zinc not only affects neighboring endocrine cells, but also plays an important role as an endogenous molecular switch that regulates the pre-meal to postprandial insulin clearance rate by the liver. Corelease of zinc and insulin caused a reduction in insulin degradation by the liver, which optimized the delivery of insulin to its peripheral target tissues.

Results

Characterization of β cell–specific ZnT8-deficient mice. To determine the role of ZnT8, we crossed *Slc30a8*$^{f/f}$ mice (which served as controls) with *Rip-cre* mice, generating *Slc30a8*$^{f/f}$*:Rip-cre* mice with β cell–specific ZnT8 deficiency (referred to herein as ZnT8KO mice) (Figure 1A). Because it is known that the zinc-binding residues are highly con-

Conflict of interest: The authors have declared that no conflict of interest exists.
Citation for this article: *J Clin Invest.* 2013;123(10):4513–4524. doi:10.1172/JCI68807.

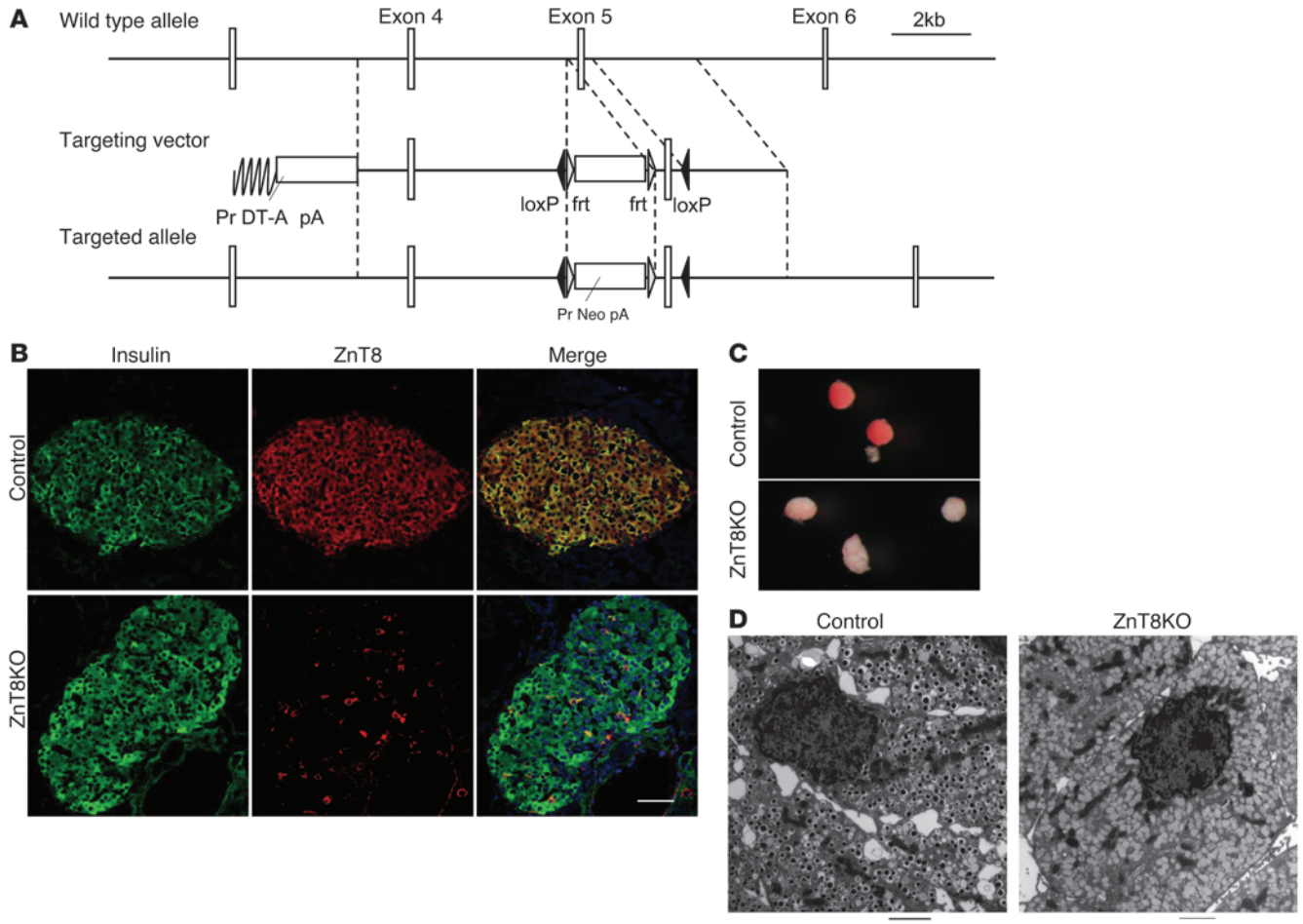

Figure 1
Generation of ZnT8KO (β cell–specific ZnT8-deficient) mice. (**A**) Generation of control *Slc30a8*$^{f/f}$ mice. (**B**) Immunohistochemical analysis of the pancreas of control and ZnT8KO mice. The pancreas was immunostained for insulin (green) and ZnT8 (red). (**C**) Dithizone staining of islets of control and ZnT8KO mice. (**D**) Electron microscopic images of β cells. Scale bars: 50 μm (**B**); 2 μm (**D**). For **C**, information on magnification was not available.

served among ZnT families and plays a critical role in zinc transporter function (6, 30, 31), our *Slc30a8*$^{f/f}$ control was designed to have deleted exon 5, which encodes a domain containing zinc-binding residues (30). ZnT8 expression was essentially absent in ZnT8KO mice (Figure 1B), and such deficiency was associated with low zinc contents in β cells, insulin crystallization failure, and presence of atypical insulin granules that lacked a detectable dense core in β cells (Figure 1, C and D). While some reports showed that insulin granules of ZnT8-deficient mice still contain dense core granules or abnormal rod-shaped insulin crystals (20, 21), our ZnT8KO mice showed almost complete loss of insulin crystals at 6 and 20 weeks of age (Figure 1D and data not shown). The characteristic of the dense core in our ZnT8KO mice was consistent with that reported by others (18, 19). i.p. GTT demonstrated that ZnT8KO mice had mildly impaired glucose tolerance with low peripheral insulin levels (Figure 2A and Supplemental Figure 1A; supplemental material available online with this article; doi:10.1172/JCI68807DS1). There were no obvious differences in body weight, insulin tolerance test, relative β cell area, or vessel structure/counts in islets between control and ZnT8KO mice (Supplemental Figure 1, B–F).

Insulin secretion and hepatic insulin clearance. Low peripheral insulin levels generally suggest low insulin secretion from the islets. Unexpectedly, however, insulin secretion from isolated ZnT8KO islets was about twice that of control islets (Figure 2B and Supplemental Figure 2A). To investigate whether the enhanced insulin secretion in ZnT8KO mice occurred within a physiological context, pancreas perfusion was performed, and enhanced insulin secretion was still noted in ZnT8KO mice (Figure 2, C and D). Because there were no differences in the vessel structure/counts in islets between control and ZnT8KO mice (Supplemental Figure 1, E and F), these results are indicative of enhanced β cell insulin secretion in ZnT8KO mice. Although previous reports described high insulin secretion from isolated ZnT8-deficient islets and low peripheral insulin (19), the mechanism of this discrepancy has not been investigated. Therefore, we next measured insulin levels before and after liver passage by performing pancreas-liver perfusion (Figure 2, E and F). Interestingly, the insulin level in the inferior vena cava (IVC) of ZnT8KO mice during pancreas-liver perfusion was comparable to that of control mice (Figure 2F). The difference in insulin level between PV and IVC (Figure 2, D and F) suggests that a large portion of the secreted insulin in ZnT8KO mice was degraded through a single liver passage.

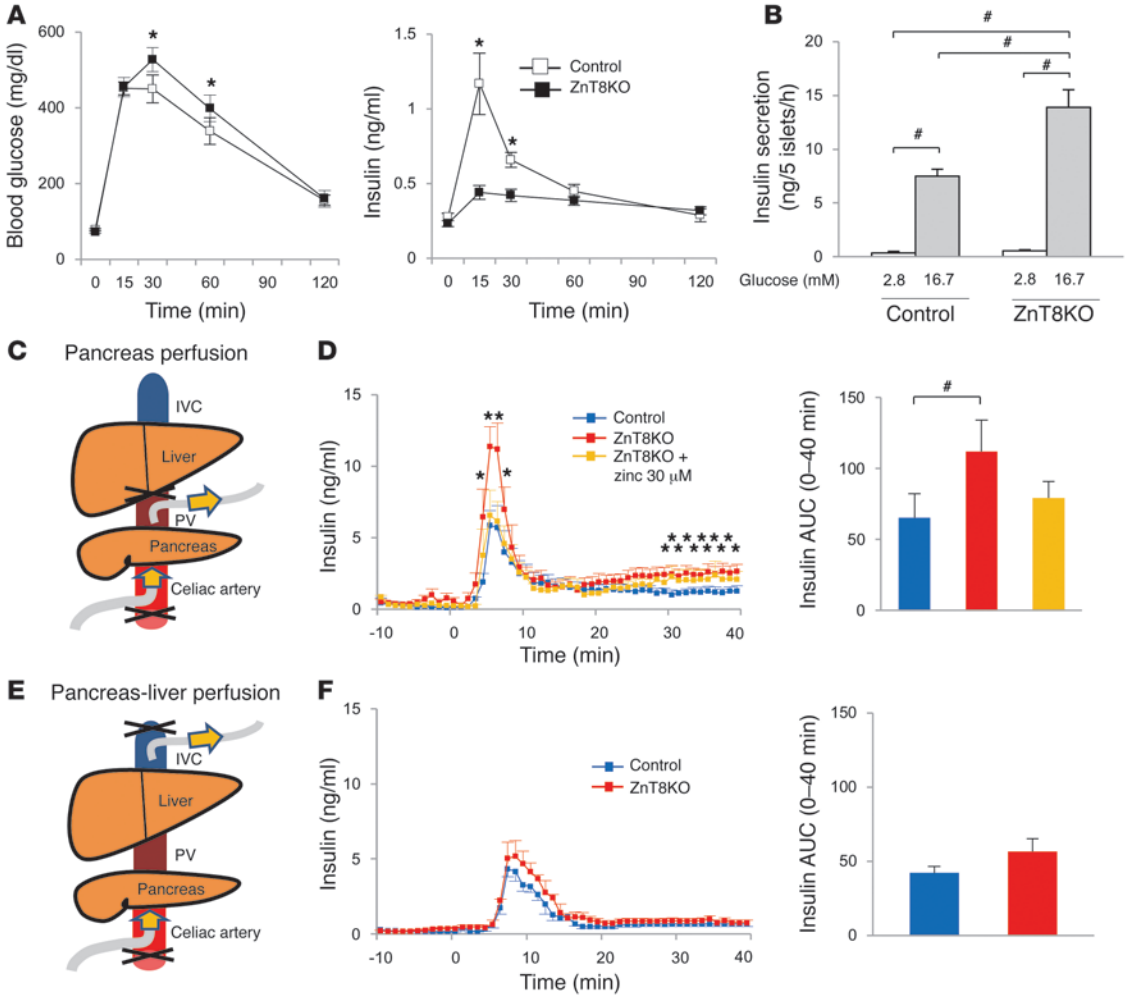

Figure 2
Characteristics of ZnT8KO mice. (**A**) Blood glucose and insulin levels during i.p. GTT in control (n = 12) and ZnT8KO (n = 11) mice. (**B**) Insulin secretion from isolated islets incubated with 2.8 or 16.7 mM glucose (n = 9 per group). (**C**) Pancreas perfusion. The perfusate was infused into the celiac artery and collected from the PV. (**D**) Insulin secretion during pancreas perfusion in controls (n = 7), ZnT8KO mice (n = 7), and ZnT8KO mice perfused with 30 μM zinc-supplemented perfusate (n = 5). (**E**) Pancreas-liver perfusion. The perfusate was infused into the celiac artery and collected from the IVC. (**F**) Insulin levels during pancreas-liver perfusion of control and ZnT8KO mice (n = 5 per group). All data are mean ± SEM. *P < 0.05 vs. control, unpaired t test. #P < 0.05, nonrepeated ANOVA.

In vivo assessment of hepatic insulin clearance in ZnT8KO mice. We next examined insulin dynamics during i.p. GTT in mice (Figure 3, A–D). Although blood insulin levels were lower in ZnT8KO mice, c-peptide levels were higher than in controls (Figure 3, A and B), consistent with hypersecretion from the ZnT8KO pancreas. The c-peptide/insulin ratio, a marker of insulin clearance (27, 32), was similar in ZnT8KO and control mice in the fasting state, but significantly higher in ZnT8KO mice at 15 and 30 minutes of i.p. GTT (Figure 3C), which suggests that insulin clearance in ZnT8KO mice is accelerated relative to controls after glucose challenge, presumably due to *Slc30a8* deficiency.

Failure of suppression of insulin clearance in humans with the SLC30A8 risk allele. As an extension of the above findings, we compared insulin clearance in 2 groups of human volunteers with normal glucose tolerance: those carrying the risk allele of *SLC30A8*, rs1366642 (C/C; n = 12), and those with a nonrisk allele (T/T or T/C; n = 42). Because we previously found that hyperglycemia downregulated ZnT8 expression in mice (33), 3 participants with impaired glucose tolerance were excluded. The clinical background of the participants was similar (Table 1). Oral GTT showed no difference in the area under the curve (AUC) for both insulin and glucose, but the AUC for c-peptide was significantly higher in the risk versus the nonrisk allele group (Figure 4, A–F). Moreover, the c-peptide/insulin ratio at 30 minutes was significantly higher in the risk versus the nonrisk allele group (Figure 4G), similar to the results in mice. Similar results were obtained comparing the T/T and C/C alleles (Supplemental Figure 3). Although it is widely accepted that enhanced insulin resistance is associated with impaired insulin clearance (29, 34), the glucose infusion rate (GIR) at each step during a glucose clamp study was similar between the nonrisk and risk groups (Figure 4H). There was no difference in intrahepatic lipid, which is known as a surrogate marker of hepatic insulin resistance, between the nonrisk and risk groups (Table 1). These findings suggest that the difference in the c-peptide/insulin ratio

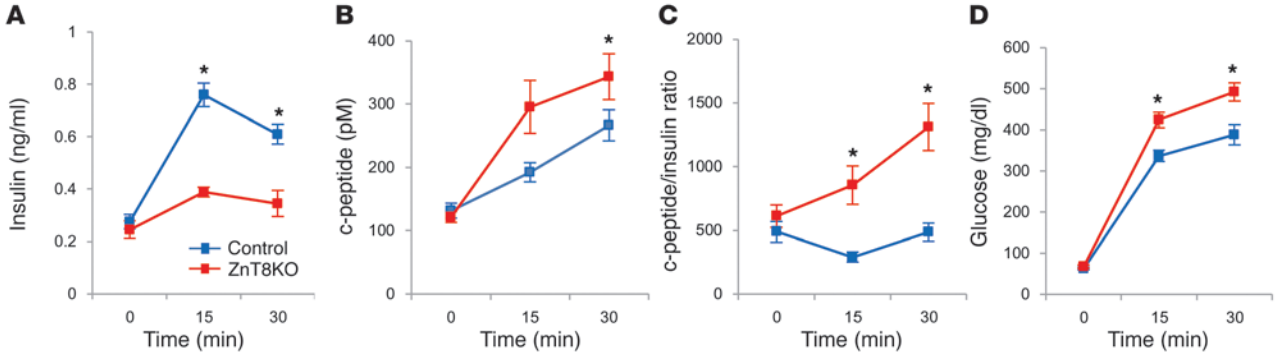

Figure 3
c-peptide/insulin ratio in ZnT8KO and control mice. (**A**) Insulin concentration, (**B**) c-peptide concentration, (**C**) c-peptide/insulin ratio, and (**D**) glucose concentration during i.p. GTT in control and ZnT8KO mice (n = 12 per group). Data are mean ± SEM. *P < 0.05, unpaired t test.

between the nonrisk and risk groups was not due to a difference in insulin resistance. In addition, the metabolic clearance rate for insulin (MCR-I) (35), represented by the clearance rate of exogenously infused insulin, was similar in the 2 groups (Figure 4I). This finding suggests that *SLC30A8* alters the insulin clearance rate of endogenously secreted insulin. In addition, we calculated the insulinogenic index, a marker of insulin secretory capacity. The insulinogenic index tended to be higher in the nonrisk allele group than the risk group (Figure 4J), which suggests that ZnT8 deficiency affects insulin levels available for insulin-sensitive tissues rather than insulin resistance. Together, the above results indicate impaired suppression of postprandial insulin clearance in humans carrying the risk allele of *SLC30A8*.

ZnT8 dependence of zinc and insulin cosecretion. Because the major differences in insulin secretion and hepatic insulin clearance were possibly related to ZnT8 function, we measured zinc content in isolated islets of control and ZnT8KO mice. As expected, ZnT8KO islets contained less zinc than control islets (Figure 5A). Zinc content per individual islet, as measured by the wet ashing method, was 21.0 ± 1.1 pmol in control mice and 6.3 ± 0.4 pmol in ZnT8KO mice, and by the nitric acid method was 36.4 ± 1.5 and 10.4 ± 0.3 pmol, respectively. While the presumed function of *Slc30a8* is to transport zinc ion into insulin granules, the difference in zinc content per islet of control and ZnT8KO mice likely represents the zinc content in insulin granules. The putative zinc content in insulin granules of a single islet accounted for 14.8 pmol (wet ashing method) to 26.1 pmol (nitric acid method). On the other hand, the insulin content of a single islet was approximately 7 pmol (40 ng) in our experiments (Supplemental Figure 2). Because insulin crystals typically consist of 2 zinc molecules and 6 insulin molecules, these findings indicate that the zinc/insulin molecular ratio is 2:1 to 4:1, generally consistent with previous reports (36, 37). This finding indicates the presence of larger amounts of zinc, which is required to form insulin hexamer (2:6 zinc/insulin), in insulin granules. In addition, we investigated whether a bolus zinc secretion into the PV could be detected as a transient rise in zinc concentration. Indeed, the zinc concentration in the PV of control mice after 2–4 minutes of glucose loading was significantly higher than in the control IVC or in the ZnT8KO IVC or PV (Figure 5B).

Based on the clear differences in zinc content and secretion between ZnT8KO and control mice, we propose the following 2 scenarios: first, zinc secreted from neighboring β cells suppresses insulin secretion from normal islets; and second, zinc released from the pancreas suppresses hepatic insulin clearance. The next series of experiments was designed to test these scenarios.

Zinc-induced suppression of insulin secretion from β cells. Zinc secreted from β cells is known to affect neighboring endocrine cells (7, 11). Consistent with previous reports (10, 14–16), addition of zinc to the perfusate (30 μM) markedly suppressed insulin hypersecretion in ZnT8KO mice, almost to control levels (Figure 2D). Furthermore, the addition of zinc chelator calcium EDTA (2.5 mM) (7) significantly increased insulin secretion from isolated C57BL/6J islets (Figure 5C and Supplemental Figure 2B).

Previous studies showed that zinc hyperpolarizes pancreatic β cells by enhancing the outward current of the K-ATP channel (8, 9). We found that insulin secretion from isolated ZnT8KO islets incubated with KCl, a K-ATP channel–independent insulin secretagogue, was comparable to that from control islets (Figure 5D and Supplemental Figure 2C), which indicates that lack of zinc secretion from β cells causes K-ATP channel–dependent insulin hypersecretion in ZnT8KO mice.

Zinc-induced suppression of hepatic insulin clearance. We next examined whether zinc released from the pancreas suppresses hepatic insulin clearance. Injection of a zinc-insulin solution into the PV resulted in reduced hepatic insulin clearance, and the reduction was zinc dose dependent (Figure 6A). To assess the regulatory role of zinc in hepatic insulin clearance directly, we performed liver perfusion experiments (Figure 6B). Zinc supplementation significantly increased insulin level in the IVC (Figure 6C), which confirmed that zinc affects hepatic insulin clearance. Moreover, insulin consumption in cultures of HepG2 cells, assessed by the concentration of insulin in the medium, also correlated negatively with zinc concentration (Figure 6D).

Zinc-induced suppression of insulin receptor internalization. Hepatic insulin clearance involves several processes, including the binding of insulin to the insulin receptor (IR), internalization of the insulin-IR complex, and proteolytic degradation by a specific insulin-degrading enzyme (IDE) (38). Since IDE is a zinc metallopeptidase (38), we first examined the effect of zinc on IDE activity. However, increasing zinc levels did not affect IDE-mediated insulin degradation in an IDE activity assay (Supplemental Figure 4). Because zinc (75–225 μM) inhibits the internalization of asialoglycoprotein and transferrin receptor (TfR) in hepatocytes (39), we next examined whether zinc chloride at 30–100 μM, concentrations used in zinc-related research in hepatocytes and liver-

Table 1
Characteristics of the nonrisk and risk allele groups

	Risk[A]	Nonrisk[B]	*P*
Age (yr)	44.1 (3.1)	42.5 (4.5)	0.71
Body mass index (kg/m^2)	24.0 (1.3)	23.9 (1.2)	0.5
Waist circumference (cm)	85.3 (5.7)	84.2 (5.1)	0.24
Systolic blood pressure (mmHg)	129.9 (17.4)	125.4 (10.7)	0.27
Diastolic blood pressure (mmHg)	82.1 (13.0)	81.8 (9.5)	0.91
HbA1c (%)	5.4 (0.4)	5.4 (0.38)	0.81
Total cholesterol (mg/dl)	206.3 (34.2)	204.4 (33.0)	0.87
Triglyceride (mg/dl)	142.0 (62.6)	145.3 (97.1)	0.91
LDL-cholesterol (mg/dl)	120.4 (28.6)	122.6 (29.5)	0.82
HDL-cholesterol (mg/dl)	60.4 (16.0)	59.1 (16.0)	0.95
Free fatty acids (μEq/l)	378.8 (97.9)	419 (136.3)	0.35
Body fat (%)	22.2 (5.6)	21.8 (4.3)	0.82
Intrahepatic lipid (%)	3.5 (3.2)	4.3 (4.8)	0.58
AST (IU/l)	23.4 (5.0)	25.3 (12.1)	0.59
ALT (IU/l)	24.2 (5.4)	35.1 (32.0)	0.23
γ-GTP (IU/l)	37.1 (16.7)	79.9 (109.3)	0.16
Procollagen III peptide (ng/ml)	0.46 (0.05)	0.48 (0.05)	0.26
Collagen type IV (ng/ml)	114.9 (21.5)	111.07 (27.1)	0.65
Hyaluronic acid (U/ml)	15.2 (7.4)	12.7 (6.7)	0.26

[A]C/C (n = 12). [B]T/T or T/C (n = 42). Data represent mean (SD). *P* values were determined by unpaired *t* test.

derived cell lines (40–46), alters insulin-stimulated internalization of the insulin-IR complex in HepG2 cells. We examined this using the biotin-labeled IR internalization assay, which measures biotin-labeled cell surface IR, but does not detect internalized or intracellular IR, thus assessing insulin-induced IR internalization from the cell surface to the cytoplasm (32, 47). Insulin stimulation decreased cell surface IR, which was suppressed by cotreatment with zinc (Figure 6E). These results suggest that zinc inhibits insulin-stimulated IR internalization. Furthermore, the zinc ionophore pyrithione enhanced, whereas the zinc chelator TPEN abolished, zinc-induced inhibition of IR internalization (Figure 6F), which suggests that the zinc-dependent inhibition of IR internalization is induced by intracellular zinc influx, rather than by zinc-sensing receptors such as GPR39 (10). To investigate the transporter responsible for the zinc influx, we examined ZIP14-deficient mice (41, 48). However, hepatic insulin clearance was not altered by ZIP14 deficiency in the liver perfusion reaction (data not shown). Collectively, these findings indicate that zinc-induced inhibition of hepatic insulin uptake involves blockade of insulin-stimulated internalization of the insulin-IR complex via ZIP14-independent intracellular zinc influx.

There are several forms of endocytosis, including the clathrin-mediated and caveolin-mediated forms (49, 50). Since transferrin (Tf) bound to TfR is internalized in a mainly clathrin-dependent manner (51), and TfR internalization is suppressed by zinc (39), we first examined the effect of zinc on Tf bound to its TfR using chlorpromazine, an inhibitor of clathrin-dependent endocytosis (52), and MβCD, an inhibitor of caveolin-dependent endocytosis (53). Confocal microscopic analyses showed that in HepG2 cells, chlorpromazine strongly suppressed the internalization of Alexa Fluor 594–conjugated Tf, compared with a negligible effect of MβCD. The effect of zinc on TfR internalization was similar to that of chlorpromazine (Figure 7, A and B), which suggests that zinc preferentially inhibits clathrin-dependent endocytosis.

Both clathrin and caveolin-1 are involved in IR endocytosis (54–56). Therefore, we investigated the mechanism by which zinc affects IR endocytosis. Confocal microscopic analysis showed that in HepG2 cells, IR was internalized into intracellular endosomal compartments at 5 and 15 minutes after treatment with FITC-conjugated insulin (Figure 7, C and D). Both chlorpromazine and MβCD suppressed IR internalization, as did zinc treatment. Interestingly, cotreatment with zinc and chlorpromazine did not show any further suppression of IR internalization compared with either single treatment, whereas treatment with MβCD with and without zinc exhibited a significant difference 15 minutes after FITC-insulin treatment (Figure 7D). Moreover, caveolin-1 phosphorylation, which is associated with caveolin-dependent endocytosis (55), was not affected by zinc supplementation (Supplemental Figure 5). These results suggest that zinc mainly inhibits clathrin-dependent, rather than caveolin-mediated, IR endocytosis. Taken together, these findings indicate that zinc suppresses IR endocytosis by inhibiting the clathrin-mediated receptor internalization machinery.

Lack of evidence of liver dysfunction in association with ZnT8 deficiency. It is possible that increased hepatic insulin internalization caused by ZnT8 deficiency could affect liver function. To rule out this possibility, a series of biochemical tests of carriers for *SLC30A8* risk allele were conducted (Table 1). The results showed that the liver function of individuals carrying the *SCL30A8* risk allele was comparable to that of individuals carrying nonrisk alleles. Next, we conducted blood tests in ZnT8KO mice at 25 weeks of age to investigate whether ZnT8 deficiency is associated with liver dysfunction. All biochemical markers related to liver function were within the normal range (Supplemental Table 1). Furthermore, the results showed neither fatty liver, fibrotic changes, nor enhanced storage of glycogen in the liver of control and ZnT8KO mice, as assessed by H&E, AZAN, and PAS staining, respectively (Supplemental Figure 6).

Little effect of proinsulin on hepatic insulin clearance. Because proinsulin secretion is reported to be increased in ZnT8KO mice and individuals carrying the risk allele of *SLC30A8* (20, 57), we investigated the role of proinsulin in the regulation of hepatic insulin clearance. First, we measured plasma proinsulin levels in ZnT8KO mice after glucose challenge and proinsulin content in control and ZnT8KO mice (Supplemental Figure 7, A–F). In agreement with a previous report (20), the proinsulin/insulin ratio was significantly higher in ZnT8KO than control mice. Proinsulin is known to bind to the IR and elicits acute insulin-like metabolic effects in adipocytes and hepatocytes, although the binding affinity to IR is 10- to 100-fold lower (58, 59). To investigate the possible role of proinsulin in the regulation of hepatic insulin clearance, we tested whether proinsulin interferes with the internalization of FITC-insulin into HepG2 cells (Supplemental Figure 7, G and H). Preincubation of HepG2 cells with 10 nM proinsulin (representing the same amount of FITC-insulin) did not affect the uptake of FITC-insulin by HepG2 cells. Given that the binding affinity of proinsulin to the IR is low, the result that proinsulin did not affect FITC-insulin endocytosis appeared to be reasonable. In addition, there was only 5% difference in the proinsulin/insulin ratio between control and ZnT8KO mice. Thus, it is unlikely that proinsulin produced in ZnT8KO islets plays a major role in the regulation of hepatic insulin clearance.

ZnT8 deficiency does not induce changes in glucagon secretion. Cross-regulation of insulin and glucagon secretion has been previously reported: insulin suppresses glucagon secretion (60), and gluca-

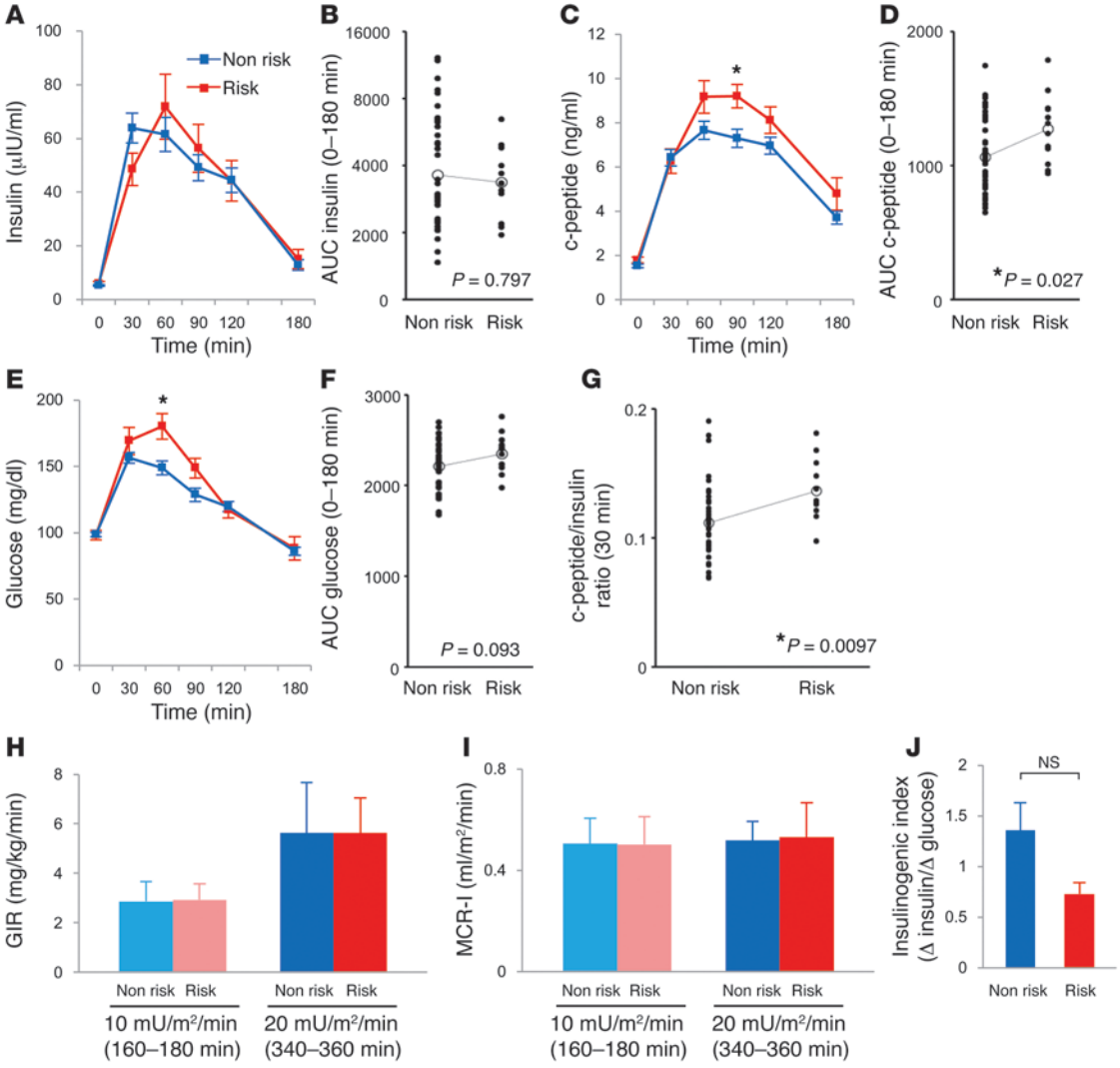

Figure 4

Increased insulin clearance in humans with the risk allele of *SLC30A8*. (**A**–**F**) Concentration (**A**, **C**, and **E**) and AUC 0–180 minutes (**B**, **D**, and **F**) of insulin (**A** and **B**), c-peptide (**C** and **D**), and glucose (**E** and **F**) during 75-g oral GTT in human nonrisk (n = 42) and risk (n = 12) allele groups. (**G**) c-peptide/insulin ratio at 30 minutes of human 75-g oral GTT. (**H**) GIR during glucose clamp at each insulin infusion rate. (**I**) MCR-I at steady state during the infusion of exogenous insulin at 10 or 20 mU/m²/min. (**J**) Insulinogenic index, calculated as change in insulin (0–30 minutes) relative to change in glucose (0–30 minutes). Data are mean ± SEM (**A**, **C**, **E**, and **J**) or mean ± SD (**H** and **I**). *P < 0.05, unpaired t test.

gon enhances insulin secretion (61). In addition, whether zinc suppresses glucagon secretion (7, 62, 63) or not (64) is currently an active area of debate. If zinc suppresses glucagon secretion, it could indirectly affect insulin secretion. Glucagon secretion was measured as described previously (19) from islets of control and ZnT8KO mice (Supplemental Figure 8, A–D). We also measured changes in plasma glucagon levels associated with glucose-stimulated insulin and zinc cosecretion in control and ZnT8KO mice, to evaluate whether loss of zinc secretion alters glucagon secretion from α cells (Supplemental Figure 8E). Consistent with the results described previously (19), glucagon secretion was similar in control and ZnT8KO mice.

Effect of high-fat diet on hepatic insulin clearance. Finally, we investigated whether high-fat diet affects hepatic insulin extraction. Mice at 8–12 weeks of age were fed high-fat diet, then evaluated for c-peptide/insulin ratio (Supplemental Figure 9, A–F). Body weight increased significantly after high-fat diet feeding in both control and ZnT8KO mice, compared with normal chow diet (Supplemental Figure 1B and Supplemental Figure 9, A and B). The c-peptide/insulin ratio was still significantly higher in ZnT8KO than control mice (Supplemental Figure 9, C–F). These results suggest that high-fat diet did not affect ZnT8-mediated suppression of hepatic insulin clearance. In addition, glucose tolerance and body weight of ZnT8KO and control mice were comparable after a longer period of high-fat diet feeding (Supplemental Figure 9, G–I). These results are consistent with those of previous reports that systemic ZnT8KO mice showed more weight gain and glucose intolerance compared with controls (18, 19, 65), but these differences were not evident in our ZnT8KO mice.

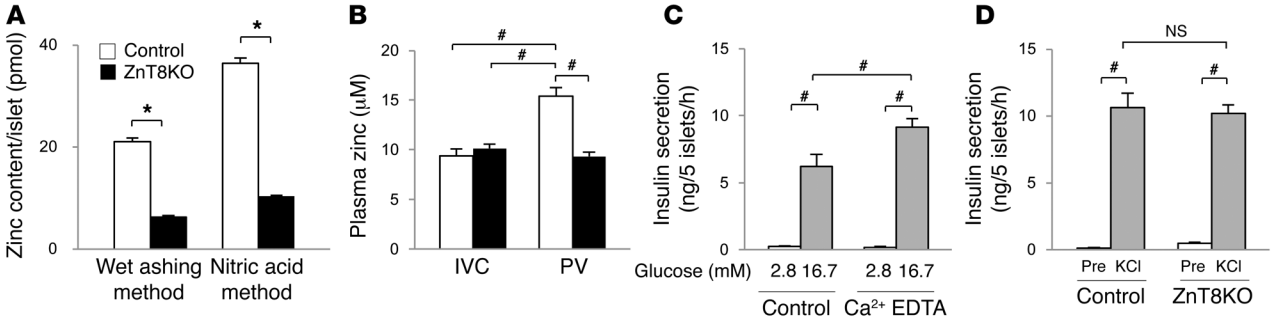

Figure 5

Zinc secreted from islets suppresses insulin secretion. (**A**) Zinc content in islets isolated from control and ZnT8KO mice, measured by the wet ashing and nitric acid methods. (**B**) Plasma zinc concentrations in the IVC and PV of control and ZnT8KO mice 2–4 minutes after i.v. glucose. (**C**) Insulin secretion from isolated C57BL6/J islets incubated with 2.8 mM glucose (n = 8 each) and 16.7 mM glucose (n = 12 each) with or without 2.5 mM Ca^{2+} EDTA. (**D**) Insulin secretion from isolated islets incubated with 2.8 mM glucose (Pre) and 50 mM KCl (n = 7 per group). All data are mean ± SEM. *P < 0.05, unpaired t test. #P < 0.05, nonrepeated ANOVA.

Discussion

In the EUGENE2 study, human homozygous carriers of the risk allele of *SLC30A8* had low peripheral insulin levels in the early phase of i.v. GTT (22). However, in 5 previous papers that characterized ZnT8-deficient mice, there was no agreement on the underlying mechanism by which *Slc30a8* increases susceptibility to type 2 diabetes (17–21). Our detailed examination of ZnT8KO mice and of humans with the R325W polymorphism of *SLC30A8* indicated that the phenotype of ZnT8 deficiency shows apparent discrepancy between insulin secretion from the pancreas and circulating insulin levels, resulting from a difference in insulin clearance. Indeed, healthy humans with the R325W polymorphism of *SLC30A8* displayed normal glucose tolerance because they maintained postprandial plasma insulin at levels similar to those of the nonrisk allele group, by secreting more insulin to overcome the enhanced hepatic insulin degradation. Since there was no difference in insulin resistance between the risk and nonrisk groups (Figure 4H), the difference in insulin clearance between groups was not related to insulin resistance. Thus, dysregulation of insulin clearance by the liver associated with the *SLC30A8* mutation may cause persistent enhancement of insulin secretion from β cells, which could increase the risk for the development of type 2 diabetes.

In general clinical practice, hypoinsulinemia is interpreted to result from low insulin secretion by pancreatic β cells. However, this cannot be confirmed without measuring insulin secretion from the pancreas, because insulin level in the systemic circulation is determined by a balance between insulin secretion and insulin clearance. The results of the EUGENE2 study are generally consistent with our results (22); hypoinsulinemia might be explained by accelerated hepatic insulin clearance. Measurement of c-peptide level and the c-peptide/insulin ratio would confirm this possibility.

Although insulin granules are known to contain high amounts of zinc, there is little information about the physiological significance of zinc. In this study, we demonstrated that the high amount of zinc contained in insulin granules and its cosecretion with insulin had endocrine functions in addition to their intracellular roles in insulin molecule crystallization and efficient insulin processing (20). First, zinc secreted from β cells inhibited insulin secretion in autocrine and paracrine fashions. Second, zinc that was cosecreted with insulin regulated postprandial hepatic insulin clearance (Supplemental Figure 10). Based on these findings, we propose the involvement of *SLC30A8* in the dysregulation of insulin homeostasis in humans, despite the limited number of study subjects.

In agreement with our observations, Rutter and colleagues (19) reported hypersecretion of insulin from islets of ZnT8-deficient mice, but low plasma insulin levels after glucose loading in these mice. However, in that study, the discrepancy between these 2 observations was not fully explored. Previous studies reported that insulin secretion from pancreatic islets was suppressed by zinc through enhanced outward current of the K-ATP channel (8–10, 14–16). Therefore, we rigorously examined whether zinc could suppress insulin secretion in various experimental settings, using isolated islets from ZnT8KO mice (Figure 2B and Figure 5D), the addition of zinc chelator to C57BL/6J islets (Figure 5C), and pancreas perfusion (Figure 2D), in addition to simple comparison between control and ZnT8KO mice. The results of all these experiments strongly supported the previous reports demonstrating that zinc suppresses insulin secretion from β cells (8–10, 14–16).

The liver is the main organ for insulin clearance, removing approximately 50% during the first portal passage (29, 34), but this rate is highly dependent on the state of satiation. In the fasting state, clearance of unnecessary insulin by the liver plays a major role in preventing inappropriate hyperinsulinemia (32). In the postprandial state, on the other hand, hepatic insulin degradation is inhibited to ensure a sufficient supply of insulin to the peripheral target tissues, although the underlying mechanism of this regulatory process has remained elusive (24, 28). Thus, timely inhibition of hepatic insulin clearance by zinc coreleased with insulin seems to be a rational mechanism.

Zinc-induced inhibition of insulin uptake by the liver was further confirmed by visualizing intracellular translocation of insulin. The internalization of FITC-insulin into HepG2 cells was acutely inhibited by zinc (Figure 7, C and D), which may account for the efficient inhibition of hepatic insulin clearance during the first liver passage. Insulin is delivered to the liver through the PV by pulsatile secretion. While pulsatile zinc concentration in the PV is unknown, to assess the regulatory role of zinc in insulin secretion and insulin metabolism, we used 30–100 μM of zinc, a concentration used in previous studies on zinc biology (40–46). TfR is a well-characterized receptor whose trafficking is clathrin dependent (66, 67). Our results showed that zinc effectively inhibited

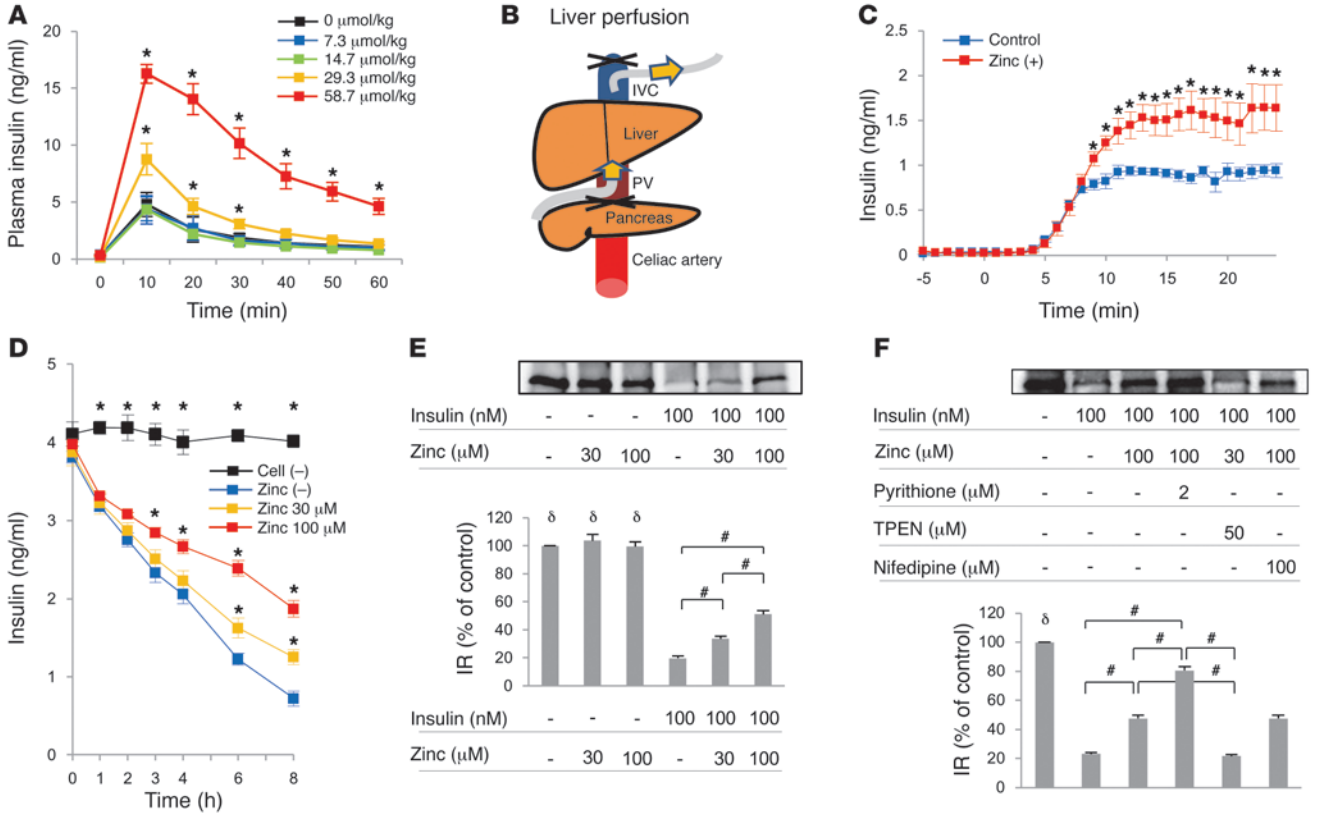

Figure 6

Zinc attenuates hepatic insulin clearance. (**A**) Peripheral insulin levels measured after intraportal coinjection of insulin and zinc, the latter at concentrations of 0, 7.3, 14.7, 29.3, or 58.7 μmol/kg body weight. (**B**) Liver perfusion. The perfusate was infused into the PV and collected from the IVC. (**C**) Liver perfusion in C57BL/6J mice ($n = 5$ per group). Blue, insulin-containing control perfusate; red, zinc-supplemented perfusate. (**D**) Insulin clearance assay. Insulin concentration was determined in the culture medium of HepG2 cells supplemented with zinc chloride at 0, 30, or 100 μM as well as in cell-free medium. (**E** and **F**) IR internalization assay. Residual IR on the cell surface was determined after administration of 100 nM insulin and/or 30 or 100 μM zinc (**E**; $n = 3$) and of insulin, zinc, pyrithione, TPEN, and/or nifedipine as indicated (**F**; $n = 5$). Percent membrane residual IR relative to control was also quantified. All data are mean ± SEM. $^{*}P < 0.05$ vs. control, unpaired t test. $^{\#}P < 0.05$ as indicated by brackets, $^{\delta}P < 0.05$ vs. all insulin treatment groups, nonrepeated ANOVA.

endocytosis of Tf (Figure 7, A and B). Zinc also further reduced IR endocytosis in the presence of MβCD, an inhibitor of the caveolin-dependent trafficking pathway, but not in the presence of chlorpromazine, an inhibitor of the clathrin-dependent trafficking pathway, which indicated that the zinc-induced suppression of IR endocytosis seems to be mediated mainly by suppression of the chlorpromazine-sensitive, clathrin-dependent pathway.

As a plausible explanation for the link between loss of ZnT8 function and enhanced hepatic insulin clearance, we postulate that zinc coreleased with insulin affects insulin degradation in the liver. Because zinc is coreleased with insulin from insulin granules of β cells, it is likely that the local zinc concentration within the insulin-containing pulsatile bloodstream is high enough to efficiently suppress insulin uptake by the IRs on hepatocytes. We cannot completely rule out the possibility that the zinc molecule binds to the secreted insulin molecules until insulin reaches the cellular surface of hepatocytes, since it takes a while for insulin crystals to dissociate and become a monomer. Based on findings from experiments involving subcutaneous insulin injection, it is believed that only insulin monomer can pass through the blood vessel wall and exist as a monomer in serum (68, 69). However, it is possible that insulin hexamers, or even crystals, may be able to pass through islet capillaries, since the endothelial cell lining of islet capillaries exhibit unique fenestration structures that allow rapid permeation of proteins (70). Because the proinsulin level relative to that of insulin was increased in ZnT8-deficient mice, we examined the possible role of proinsulin in modulating hepatic insulin clearance; however, no such evidence was obtained (Supplemental Figure 7). It is also possible that a yet-unknown substance can alter hepatic insulin clearance in association with the function of *SLC30A8* in β cells. Although such hypotheses should be verified, investigating the nature of existence of insulin molecules in the PV is beyond the reach of currently available techniques.

It has been pointed out that differences in genetic background of mice and mouse facilities could affect the phenotype of mice mutant for *Slc30a8* (21). It is thus possible that the background of our ZnT8KO mice may have contributed to the difference in mouse phenotype. In addition, the genetic background of ES cells used in our experiments was also different. We used TT2 ES cells, in contrast to the 129/Sv^{EvBrd} cells used by Pound and colleagues (17, 21) and the 129/SV cells used by the Nicolson, Lemaire, and Wijesekara groups (18–20). Preservation of the neighboring region of *Slc30a8* on chromosome 15 is expected, in spite of backcrossing more than 10 times. These methodological differences might have contrib-

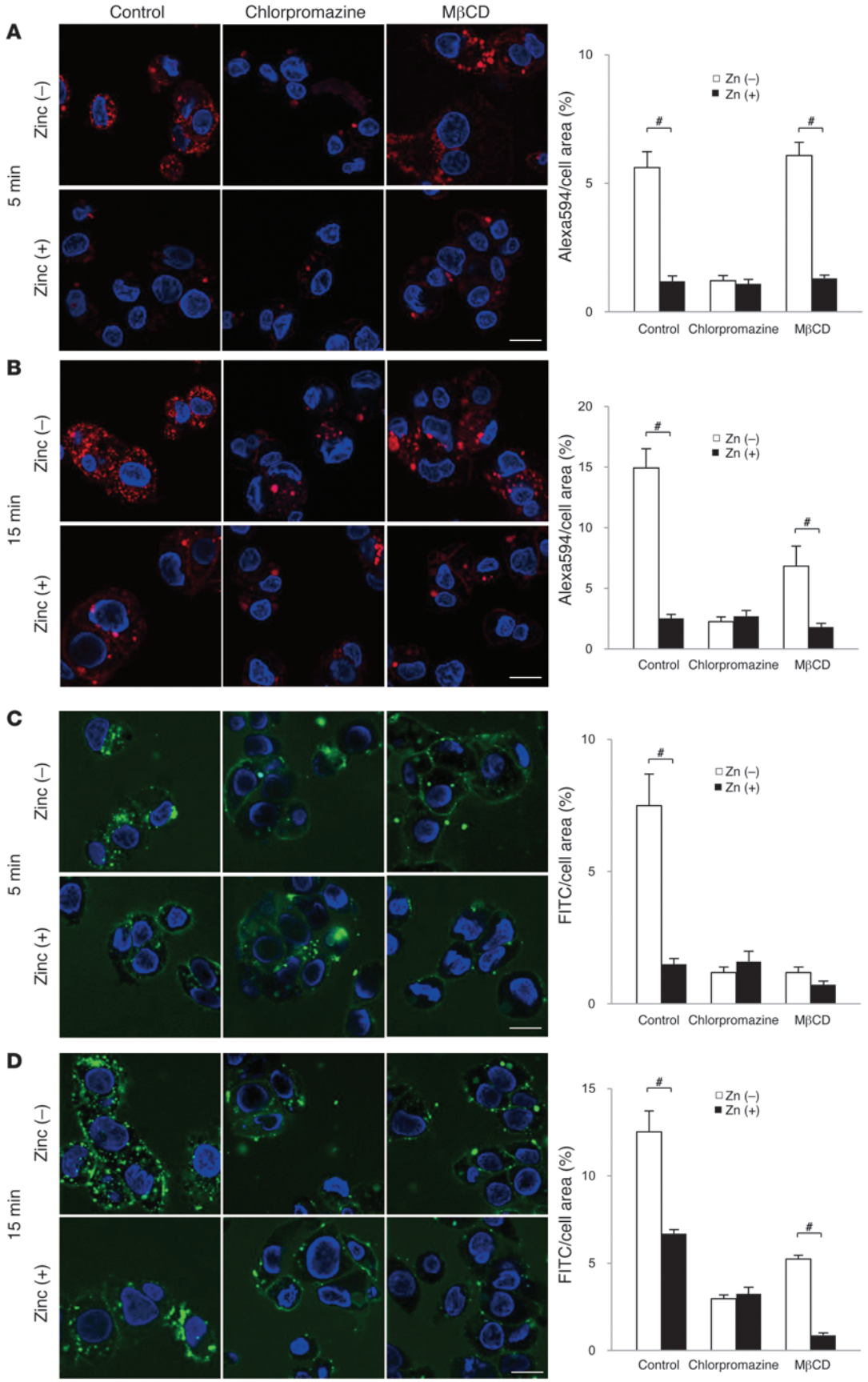

Figure 7
Zinc suppresses clathrin-mediated receptor endocytosis. (**A**–**D**) Effects of zinc on endocytosis of Alexa Fluor 594–conjugated Tf (**A** and **B**) or FITC-conjugated insulin (**C** and **D**) in HepG2 cells in the presence of chlorpromazine or MβCD at 5 (**A** and **C**) and 15 (**B** and **D**) minutes. Positive area was quantified and presented as a percentage of whole cell area. Scale bars: 10 μm. $^{\#}P < 0.05$, unpaired *t* test.

uted to the difference in mouse phenotype. Moreover, Lemaire and coworkers (71) proposed that residual zinc flux into insulin granules can be associated with the continued presence of insulin crystals, while loss of ZnT8 function and/or expression could abolish insulin crystals in ZnT8-deficient β cells. Our ZnT8KO mice showed almost complete loss of crystal-containing granules at 6 and 20 weeks of age. Based on the above hypothesis, it is likely that our mice exhibited almost complete loss of ZnT8 function. Efficient elimination of ZnT8 function might be achieved by deletion of the conserved zinc-binding residues, which are crucial for transporter function (Figure 1D and refs. 6, 30, 31). Even if truncated ZnT8 protein could be generated from the mutant allele, it contains no transporter function. Given that other groups deleted exon 1 (17, 21) or exon 3 (18–20), we cannot completely rule out the possible contribution of differences in mouse design and the degree of residual zinc flux to the different phenotypes.

The allele prevalence of the R325W polymorphism of *SLC30A8* suggests that more than one-quarter of all people may have impaired zinc secretion from the pancreas, due to genetic predisposition (1–5). In addition, our previous finding in mice of downregulated ZnT8 expression in the early stage of diabetes (33) suggests that numerous diabetic patients with hyperglycemia suffer from dysregulation of insulin clearance. Thus, our present findings provide a novel etiological concept for diabetes: dysregulated hepatic insulin clearance, which could serve as a new therapeutic target for type 2 diabetes.

Methods

Generation of ZnT8KO mice. Gene targeting in ES cells was designed to delete exon 5 of the endogenous *Slc30a8* locus (Figure 1A). The targeting vector contained exon 5 flanked by loxP sites and an *frt*-flanked neocassette (*Pr-Neo pA*) in the 3′-adjacent region. Vector electroporation into TT2 ES cells (72), positive-negative selection, and Southern blot analysis (data not shown) yielded frt-Neo^r heterozygous ES cell clones. These cells were injected into CD-1 8-cell-stage embryos to generate chimeric mutant mice. The neocassette was excised in vivo by crossing the chimeras to mice expressing the Flp recombinase (B6-Tg [CAG-FLPe36]; ref. 73), leading to *Slc30a8*$^{f/+}$ offspring (accession no. CDB0625K; http://www.cdb.riken.jp/arg/mutant%20mice%20list.html). *Slc30a8*$^{f/+}$ mice were then backcrossed onto the C57BL6/J background more than 10 times. The resulting *Slc30a8*$^{f/f}$ mice were bred with *RIP-cre* transgenic mice to generate ZnT8KO mice, with β cell–specific *Slc30a8* deletion. Mice were housed in a specific pathogen–free facility and maintained on normal mouse chow. All mice were housed in specific pathogen–free barrier facilities, maintained under a 12-hour light/12-hour dark cycle, fed standard rodent food (Oriental Yeast) or rodent food containing 60% fat (Research Diet) for the high-fat diet study, and provided water ad libitum.

PCR genotyping primer pair for Slc30a8$^{f/f}$ *mice*. The primer pair for *Slc30a8*$^{f/f}$ mice was as follows: 5′ primer, ACAGTGACAAAACAGTGGAACTTAC; 3′ primer, CTGAAGAAACTCAAGGTGTCCA. The PCR product of the floxed allele was 762 bp, that for the Δ allele was 308 bp, and that for the non–gene recombined C57BL/6J allele was 1,037 bp.

Immunohistochemistry. Immunohistochemical analysis, estimation of percent β cell area in the pancreas, and determination of the CD31-positive area in islets were carried out as described previously (74), using the following primary antibodies: rabbit anti-ZnT8 antibody (33), guinea pig anti-insulin antibody (Linco Research), and rat anti-CD31 antibody (Pharmingen).

Dithizone staining. Isolated islets were stained with 100 μg/ml dithizone (Sigma-Aldrich) for 15 minutes before imaging.

Electron microscopy. Electron microscopy was conducted using a standard protocol as described previously (75).

i.p. GTT. Male mice were fasted overnight, then loaded with 2.0 g/kg glucose. i.p. GTT was performed as described previously (75). Insulin was measured by ultrasensitive mouse insulin ELISA (Morinaga). c-peptide was measured by mouse c-peptide ELISA (Alpco). Proinsulin was measured by mouse proinsulin ELISA (Alpco).

Glucagon secretion in vivo. Mice were fasted for 6 hours, and 2.0 g/kg glucose was administrated in control and ZnT8KO mice. After 30 minutes, blood was collected from the IVC and mixed with aprotinin-EDTA. The blood samples were immediately centrifuged, and plasma was stored in a deep freezer. Glucagon level was measured by Rat, Mouse and Human Glucagon EIA kit.

Insulin tolerance test. Mice were fasted overnight, then injected with 0.75 U/kg human insulin (Eli Lilly). Blood glucose was measured in blood samples obtained from the tail vein (75).

Insulin and glucagon secretion from isolated islets. Pancreatic islets were isolated from 14- to 16-week-old male mice by collagenase digestion. Insulin secretion from isolated islets and insulin content of islets were assessed as described previously (75). Glucagon secretion and content were measured as described previously (19).

Pancreas perfusion and pancreas-liver perfusion. Overnight-fasted 14- to 16-week-old male mice were used in perfusion experiments, which were conducted as described previously (76). Briefly, after anesthetization with sodium pentobarbital, the superior mesenteric and renal arteries were ligated, and the aorta was tied off just below the diaphragm. The perfusate was infused through a catheter placed in the abdominal aorta and collected from the PV or IVC. The caudal vena cava (at the level of the inferior border of the liver) was ligated when the perfusate was collected from the IVC to avoid interfusion from other organs. The perfusate was mixed with Krebs-Ringer bicarbonate HEPES (KRBH) buffer supplemented with 4.6% dextran and 0.25% BSA and bubbled with a 95% O_2–5% CO_2 gas mixture. The flow rate of the perfusate was set at 1 ml/min. In the experiments, KRBH buffer containing 2.8 mM glucose was perfused for 15 minutes (i.e., equilibration period), and then KRBH buffer containing 16.7 mM glucose, with or without 30 μM zinc chloride, was perfused for 45 minutes. During the perfusion period, the mouse body was kept at 37°C with normal saline.

Measurement of insulin clearance in humans. 57 nondiabetic (fasting blood glucose, <126 mg/dl) men were recruited for a study performed at the Sportology Center of Juntendo University. Each subject underwent 2-step euglycemic hyperinsulinemic glucose clamp (see below), proton-magnetic resonance spectroscopy (MRS) to measure intrahepatic lipid, and 75-g oral GTT. To avoid instrument-related measurement errors, all studies were conducted at Juntendo University. The risk allele of *SLC30A8*, rs1366642, was determined by TaqMan SNP genotyping (Applied Biosystems). We divided the subjects into nonrisk allele (T/C and T/T, n = 42) and risk allele (C/C, n = 12) groups, or into T/T allele (n = 19) and C/C allele (n = 12) groups.

2-step euglycemic hyperinsulinemic glucose clamp study. After an overnight fast, a 2-step euglycemic hyperinsulinemic glucose clamp study was performed. Briefly, an i.v. cannula was placed in each forearm, and subjects received insulin infusions of 10 and 20 mU/m^2/min. Each insulin infusion step lasted 3 hours. A variable rate of infusion was used for 20% glucose to maintain euglycemia (target blood glucose, ~95 mg/dl). We used the GIR at each step as an index of insulin sensitivity. MCR-I was calculated as described previously (35).

Zinc content in islets. 50 islets from control and ZnT8KO mice were collected into 2.0-ml microtubes. Islets were homogenized by ultrasonic treatment and diluted in 200 μl distilled water. Zinc concentration in islets was measured by the wet ashing method or nitric acid method at the Sino-test Science Laboratory.

Serum zinc measurement. Mice were fasted overnight, then anesthetized and injected with glucose at 2.0 g/kg body weight via the IVC. Blood was collected from the PV 2–4 minutes later, or from the IVC 10 minutes later. Blood samples were centrifuged immediately, and plasma samples were stored until measurement of insulin concentration. Plasma zinc concentration was measured by atomic absorption spectrometry using a clinical chemistry autoanalyzer (Hitachi autoanalyzer 7180) at the Sino-test Science Laboratory.

Insulin clearance in vivo. C57BL6/J mice were fasted overnight, then anesthetized with sodium pentobarbital, followed by injection of insulin solution (0.5 U/kg body weight) mixed with various concentrations of zinc (7.3, 14.7, 29.3, or 58.7 μmol/kg body weight) into the PV. Blood samples were collected from the tail vein. Insulin levels were measured at 0, 10, 20, 30, 40, 50, and 60 minutes after injection.

Liver perfusion. The perfusate was infused through a catheter placed into the PV and collected from the IVC; the caudal vena cava was tied off to avoid interfusion from other organs. The flow rate of the perfusate was set at 0.2 ml/min. KRBH buffer containing 5.0 mM glucose was perfused for 10 minutes, representing the equilibration period. This was followed by infusion of KRBH buffer supplemented with 5.0 mM glucose plus 4.0 ng/ml human insulin (Humalin R; Eli Lilly), or with 5.0 mM glucose, 4.0 ng/ml human insulin, and 30 μM zinc hydrochloride.

Cell-based insulin degradation assay. HepG2 cells were grown to subconfluence on a 6-well dish. One well was a cell-free control in each study. The appropriate amount of human insulin (Humalin R; Eli Lilly) and 0–100 μM zinc chloride were applied to the cell cultures. The medium was collected after 0, 1, 2, 3, 4, 6, and 8 hours of culture, and the insulin concentration was measured.

IR internalization assay. HepG2 cells were cultured on a 6-well dish, followed by addition of 100 nM insulin and/or 30–100 μM zinc chloride and further incubation for 10 minutes. The biotin-labeled IR internalization assay was performed as described previously (32, 47).

IDE activity assay. HepG2 cells were collected by scraping, then incubated in CytoBuster Protein extraction reagent (Novagen) for 5 or 15 minutes. IDE was quantified using the FRET substrate (Mca-GGFLRKH-GQEDDnp), a component of the InnoZymeInsulysin/IDE Immunocapture Activity Assay Kit (Calbiochem/Merck) (77, 78).

Tf and insulin uptake in HepG2 cells. Appropriate numbers of HepG2 cells were cultured on cover glasses placed in 3.5-cm dishes. Cells were cultured in HBSS medium for 30 minutes with or without 2 mM MβCD or 50 μM chlorpromazine. Cells were placed on ice, and 100 μM zinc was added to some samples. After 5 minutes on ice, insulin-FITC or Tf–Alexa Fluor 594 was administered, and the cells were incubated at 37°C in a CO_2 incubator for 5 or 15 minutes. Cells were then washed with cold PBS and fixed in 4-PFA. The cover glass was removed from the dish and observed by confocal microscopy as described previously (33).

Statistics. All quantitative data are reported as mean ± SEM or mean ± SD. Statistical analysis was performed using unpaired 2-tailed Student's *t* test or nonrepeated ANOVA. A *P* value less than 0.05 was considered statistically significant.

Study approval. Animal experiment protocols were approved by the Ethics Review Committee for Animal Experimentation of Juntendo University. All human subjects provided written informed consent, and the study was approved by the Ethics Committee of Juntendo University.

Acknowledgments

We thank W. Ogawa, K. Ueki, T. Miki, M. Hoshino, Y. Uchiyama, and M. Koike for valuable discussions; N. Daimaru, K. Nakamura, E. Magoshi, Y. Nakamichi, and N. Ohshima for excellent technical assistance; and K. Higurashi for measurement of zinc concentrations. We also acknowledge the support of the Mouse Facility and the Cell Imaging Core at Juntendo University. This work was supported by grants from the Ministry of Education, Sports and Culture of Japan (to Y. Fujitani and H. Watada), the Japan Diabetes Foundation (to Y. Fujitani), and the Astellas Foundation for Research on Metabolic Disorders (to Y. Fujitani).

Received for publication January 14, 2013, and accepted in revised form July 11, 2013.

Address correspondence to: Yoshio Fujitani, Department of Metabolism and Endocrinology, Juntendo University Graduate School of Medicine, 2-1-1 Hongo, Bunkyo-ku, Tokyo 113-8421, Japan. Phone: 81.3.5802.1579; Fax: 81.3.3813.5996; E-mail: fujitani@juntendo.ac.jp.

1. Saxena R, et al. Genome-wide association analysis identifies loci for type 2 diabetes and triglyceride levels. *Science*. 2007;316(5829):1331–1336.
2. Scott LJ, et al. A genome-wide association study of type 2 diabetes in Finns detects multiple susceptibility variants. *Science*. 2007;316(5829):1341–1345.
3. Zeggini E, et al. Replication of genome-wide association signals in UK samples reveals risk loci for type 2 diabetes. *Science*. 2007;316(5829):1336–1341.
4. Sladek R, et al. A genome-wide association study identifies novel risk loci for type 2 diabetes. *Nature*. 2007;445(7130):881–885.
5. Takeuchi F, et al. Confirmation of multiple risk Loci and genetic impacts by a genome-wide association study of type 2 diabetes in the Japanese population. *Diabetes*. 2009;58(7):1690–1699.
6. Chimienti F, Devergnas S, Favier A, Seve M. Identification and cloning of a beta-cell-specific zinc transporter, ZnT-8, localized into insulin secretory granules. *Diabetes*. 2004;53(9):2330–2337.
7. Ishihara H, Maechler P, Gjinovci A, Herrera PL, Wollheim CB. Islet beta-cell secretion determines glucagon release from neighbouring alpha-cells. *Nat Cell Biol*. 2003;5(4):330–335.
8. Bancila V, et al. Two SUR1-specific histidine residues mandatory for zinc-induced activation of the rat KATP channel. *J Biol Chem*. 2005;280(10):8793–8799.
9. Prost AL, Bloc A, Hussy N, Derand R, Vivaudou M. Zinc is both an intracellular and extracellular regulator of KATP channel function. *J Physiol*. 2004; 559(pt 1):157–167.
10. Tremblay F, et al. Disruption of G protein-coupled receptor 39 impairs insulin secretion in vivo. *Endocrinology*. 2009;150(6):2586–2595.
11. Kim BJ, et al. Zinc as a paracrine effector in pancreatic islet cell death. *Diabetes*. 2000;49(3):367–372.
12. Fu Y, et al. Down-regulation of ZnT8 expression in INS-1 rat pancreatic beta cells reduces insulin content and glucose-inducible insulin secretion. *PLoS One*. 2009;4(5):e5679.
13. Chimienti F, et al. In vivo expression and functional characterization of the zinc transporter ZnT8 in glucose-induced insulin secretion. *J Cell Sci*. 2006;119(pt 20):4199–4206.
14. Ferrer R, Soria B, Dawson CM, Atwater I, Rojas E. Effects of Zn2+ on glucose-induced electrical activity and insulin release from mouse pancreatic islets. *Am J Physiol*. 1984;246(5 pt 1):C520–C527.
15. Ghafghazi T, McDaniel ML, Lacy PE. Zinc-induced inhibition of insulin secretion from isolated rat islets of Langerhans. *Diabetes*. 1981;30(4):341–345.
16. Aspinwall CA, Brooks SA, Kennedy RT, Lakey JR. Effects of intravesicular H+ and extracellular H+ and Zn2+ on insulin secretion in pancreatic beta cells. *J Biol Chem*. 1997;272(50):31308–31314.
17. Pound LD, et al. Deletion of the mouse Slc30a8 gene encoding zinc transporter-8 results in impaired insulin secretion. *Biochem J*. 2009; 421(3):371–376.
18. Lemaire K, et al. Insulin crystallization depends on zinc transporter ZnT8 expression, but is not required for normal glucose homeostasis in mice. *Proc Natl Acad Sci U S A*. 2009;106(35):14872–14877.
19. Nicolson TJ, et al. Insulin storage and glucose homeostasis in mice null for the granule zinc transporter ZnT8 and studies of the type 2 diabetes-associated variants. *Diabetes*. 2009;58(9):2070–2083.
20. Wijesekara N, et al. Beta cell-specific Znt8 deletion in mice causes marked defects in insulin processing, crystallisation and secretion. *Diabetologia*. 2010; 53(8):1656–1668.
21. Pound LD, et al. The physiological effects of deleting the mouse slc30a8 gene encoding zinc transporter-8 are influenced by gender and genetic background. *PLoS One*. 2012;7(7):e40972.
22. Boesgaard TW, et al. The common SLC30A8 Arg325Trp variant is associated with reduced first-phase insulin release in 846 non-diabetic offspring of type 2 diabetes patients — the EUGENE2 study. *Diabetologia*. 2008;51(5):816–820.
23. Eaton RP, Allen RC, Schade DS. Hepatic removal of insulin in normal man: dose response to endogenous insulin secretion. *J Clin Endocrinol Metab*. 1983; 56(6):1294–1300.
24. Caumo A, Florea I, Luzi L. Effect of a variable hepatic insulin clearance on the postprandial insulin profile: insights from a model simulation study.

Acta Diabetol. 2007;44(1):23–29.
25. Ahren B, Thomaseth K, Pacini G. Reduced insulin clearance contributes to the increased insulin levels after administration of glucagon-like peptide 1 in mice. *Diabetologia*. 2005;48(10):2140–2146.
26. Rudovich NN, Rochlitz HJ, Pfeiffer AF. Reduced hepatic insulin extraction in response to gastric inhibitory polypeptide compensates for reduced insulin secretion in normal-weight and normal glucose tolerant first-degree relatives of type 2 diabetic patients. *Diabetes*. 2004;53(9):2359–2365.
27. Meier JJ, Holst JJ, Schmidt WE, Nauck MA. Reduction of hepatic insulin clearance after oral glucose ingestion is not mediated by glucagon-like peptide 1 or gastric inhibitory polypeptide in humans. *Am J Physiol Endocrinol Metab*. 2007;293(3):E849–E856.
28. Meier JJ, Veldhuis JD, Butler PC. Pulsatile insulin secretion dictates systemic insulin delivery by regulating hepatic insulin extraction in humans. *Diabetes*. 2005;54(6):1649–1656.
29. Polonsky KS, et al. Quantitative study of insulin secretion and clearance in normal and obese subjects. *J Clin Invest*. 1988;81(2):435–441.
30. Lu M, et al. Structure of the zinc transporter YiiP. *Science*. 2007;317(5845):1746–1748.
31. Hoch E, Lin W, Chai J, Hershfinkel M, Fu D, Sekler I. Histidine pairing at the metal transport site of mammalian ZnT transporters controls Zn2+ over Cd2+ selectivity. *Proc Natl Acad Sci U S A*. 2012; 109(19):7202–7207.
32. Poy MN, et al. CEACAM1 regulates insulin clearance in liver. *Nat Genet*. 2002;30(3):270–276.
33. Tamaki M, Fujitani Y, Uchida T, Hirose T, Kawamori R, Watada H. Downregulation of ZnT8 expression in pancreatic beta-cells of diabetic mice. *Islets*. 2009;1(2):124–128.
34. Peiris AN, Mueller RA, Smith GA, Struve MF, Kissebah AH. Splanchnic insulin metabolism in obesity. Influence of body fat distribution. *J Clin Invest*. 1986; 78(6):1648–1657.
35. Acerini CL, Cheetham TD, Edge JA, Dunger DB. Both insulin sensitivity and insulin clearance in children and young adults with type I (insulin-dependent) diabetes vary with growth hormone concentrations and with age. *Diabetologia*. 2000; 43(1):61–68.
36. Zalewski PD, et al. Video image analysis of labile zinc in viable pancreatic islet cells using a specific fluorescent probe for zinc. *J Histochem Cytochem*. 1994; 42(7):877–884.
37. Lubag AJ, De Leon-Rodriguez LM, Burgess SC, Sherry AD. Noninvasive MRI of beta-cell function using a Zn2+-responsive contrast agent. *Proc Natl Acad Sci U S A*. 2011;108(45):18400–18405.
38. Duckworth WC, Bennett RG, Hamel FG. Insulin degradation: progress and potential. *Endocr Rev*. 1998;19(5):608–624.
39. McAbee DD, Jiang X. Copper and zinc ions differentially block asialoglycoprotein receptor-mediated endocytosis in isolated rat hepatocytes. *J Biol Chem*. 1999;274(21):14750–14758.
40. Schroeder JJ, Cousins RJ. Interleukin 6 regulates metallothionein gene expression and zinc metabolism in hepatocyte monolayer cultures. *Proc Natl Acad Sci U S A*. 1990;87(8):3137–3141.
41. Liuzzi JP, et al. Interleukin-6 regulates the zinc transporter Zip14 in liver and contributes to the hypozincemia of the acute-phase response. *Proc Natl Acad Sci U S A*. 2005;102(19):6843–6848.
42. Shi X, et al. Stable inducible expression of a functional rat liver organic anion transport protein in HeLa cells. *J Biol Chem*. 1995;270(43):25591–25595.
43. Szuster-Ciesielska A, Plewka K, Daniluk J, Kandefer-Szerszen M. Zinc supplementation attenuates ethanol- and acetaldehyde-induced liver stellate cell activation by inhibiting reactive oxygen species (ROS) production and by influencing intracellular signaling. *Biochem Pharmacol*. 2009; 78(3):301–314.
44. Bremner I, Davies NT. The induction of metallothionein in rat liver by zinc injection and restriction of food intake. *Biochem J*. 1975;149(3):733–738.
45. Azriel-Tamir H, Sharir H, Schwartz B, Hershfinkel M. Extracellular zinc triggers ERK-dependent activation of Na+/H+ exchange in colonocytes mediated by the zinc-sensing receptor. *J Biol Chem*. 2004; 279(50):51804–51816.
46. Holst B, et al. GPR39 signaling is stimulated by zinc ions but not by obestatin. *Endocrinology*. 2007; 148(1):13–20.
47. Choice CV, Howard MJ, Poy MN, Hankin MH, Najjar SM. Insulin stimulates pp120 endocytosis in cells co-expressing insulin receptors. *J Biol Chem*. 1998; 273(35):22194–22200.
48. Hojyo S, et al. The zinc transporter SLC39A14/ZIP14 controls G-protein coupled receptor-mediated signaling required for systemic growth. *PLoS One*. 2011;6(3):e18059.
49. Doherty GJ, McMahon HT. Mechanisms of endocytosis. *Annu Rev Biochem*. 2009;78:857–902.
50. Schutze S, Tchikov V, Schneider-Brachert W. Regulation of TNFR1 and CD95 signalling by receptor compartmentalization. *Nat Rev Mol Cell Biol*. 2008; 9(8):655–662.
51. Liu AP, Aguet F, Danuser G, Schmid SL. Local clustering of transferrin receptors promotes clathrin-coated pit initiation. *J Cell Biol*. 2010;191(7):1381–1393.
52. Wang LH, Rothberg KG, Anderson RG. Mis-assembly of clathrin lattices on endosomes reveals a regulatory switch for coated pit formation. *J Cell Biol*. 1993;123(5):1107–1117.
53. Adebiyi A, Narayanan D, Jaggar JH. Caveolin-1 assembles type 1 inositol 1,4,5-trisphosphate receptors and canonical transient receptor potential 3 channels into a functional signaling complex in arterial smooth muscle cells. *J Biol Chem*. 2011; 286(6):4341–4348.
54. Corvera S. Insulin stimulates the assembly of cytosolic clathrin onto adipocyte plasma membranes. *J Biol Chem*. 1990;265(5):2413–2416.
55. Fagerholm S, Ortegren U, Karlsson M, Ruishalme I, Stralfors P. Rapid insulin-dependent endocytosis of the insulin receptor by caveolae in primary adipocytes. *PLoS One*. 2009;4(6):e5985.
56. Ceresa BP, Kao AW, Santeler SR, Pessin JE. Inhibition of clathrin-mediated endocytosis selectively attenuates specific insulin receptor signal transduction pathways. *Mol Cell Biol*. 1998; 18(7):3862–3870.
57. Kirchhoff K, et al. Polymorphisms in the TCF7L2, CDKAL1, and SLC30A8 genes are associated with impaired proinsulin conversion. *Diabetologia*. 2008; 51(4):597–601.
58. Peavy DE, Abram JD, Frank BH, Duckworth WC. In vitro activity of biosynthetic human proinsulin. Receptor binding and biologic potency of proinsulin and insulin in isolated rat adipocytes. *Diabetes*. 1984;33(11):1062–1067.
59. Desbuquois B, Chauvet G, Kouach M, Authier F. Cell itinerary and metabolic fate of proinsulin in rat liver: in vivo and in vitro studies. *Endocrinology*. 2003; 144(12):5308–5321.
60. Kawamori D, et al. Insulin signaling in alpha cells modulates glucagon secretion in vivo. *Cell Metab*. 2009;9(4):350–361.
61. Huypens P, Ling Z, Pipeleers D, Schuit F. Glucagon receptors on human islet cells contribute to glucose competence of insulin release. *Diabetologia*. 2000;43(8):1012–1019.
62. Slucca M, Harmon JS, Oseid EA, Bryan J, Robertson RP. ATP-sensitive K+ channel mediates the zinc switch-off signal for glucagon response during glucose deprivation. *Diabetes*. 2010;59(1):128–134.
63. Cheng-Xue R, et al. Tolbutamide controls glucagon release from mouse islets differently than glucose: involvement of K(ATP) channels from both α-cells and δ-cells. *Diabetes*. 2013;62(5):1612–1622.
64. Ravier MA, Rutter GA. Glucose or insulin, but not zinc ions, inhibit glucagon secretion from mouse pancreatic α-cells. *Diabetes*. 2005;54(6):1789–1797.
65. Hardy AB, et al. Effects of high-fat diet feeding on Znt8-null mice: differences between beta-cell and global knockout of Znt8. *Am J Physiol Endocrinol Metab*. 2012;302(9):E1084–E1096.
66. Hanover JA, Beguinot L, Willingham MC, Pastan IH. Transit of receptors for epidermal growth factor and transferrin through clathrin-coated pits. Analysis of the kinetics of receptor entry. *J Biol Chem*. 1985;260(29):15938–15945.
67. Ehrlich M, et al. Endocytosis by random initiation and stabilization of clathrin-coated pits. *Cell*. 2004;118(5):591–605.
68. Helmerhorst E, Stokes GB. Self-association of insulin. Its pH dependence and effect of plasma. *Diabetes*. 1987;36(3):261–264.
69. Kang S, Brange J, Burch A, Volund A, Owens DR. Subcutaneous insulin absorption explained by insulin's physicochemical properties. Evidence from absorption studies of soluble human insulin and insulin analogues in humans. *Diabetes Care*. 1991;14(11):942–948.
70. Lammert E, et al. Role of VEGF-A in vascularization of pancreatic islets. *Curr Biol*. 2003;13(12):1070–1074.
71. Lemaire K, Chimienti F, Schuit F. Zinc transporters and their role in the pancreatic β-cell. *J Diabetes Investig*. 2012;3(3):202–211.
72. Yagi T, et al. A novel ES cell line, TT2, with high germline-differentiating potency. *Anal Biochem*. 1993; 214(1):70–76.
73. Kanki H, Suzuki H, Itohara S. High-efficiency CAG-FLPe deleter mice in C57BL/6J background. *Exp Anim*. 2006;55(2):137–141.
74. Nakayama S, et al. Impact of whole body irradiation and vascular endothelial growth factor-A on increased beta cell mass after bone marrow transplantation in a mouse model of diabetes induced by streptozotocin. *Diabetologia*. 2009; 52(1):115–124.
75. Ebato C, et al. Autophagy is important in islet homeostasis and compensatory increase of beta cell mass in response to high-fat diet. *Cell Metab*. 2008; 8(4):325–332.
76. Miki T, et al. Distinct effects of glucose-dependent insulinotropic polypeptide and glucagon-like peptide-1 on insulin secretion and gut motility. *Diabetes*. 2005;54(4):1056–1063.
77. Pivovarova O, Gogebakan O, Pfeiffer AF, Rudovich N. Glucose inhibits the insulin-induced activation of the insulin-degrading enzyme in HepG2 cells. *Diabetologia*. 2009;52(8):1656–1664.
78. Leissring MA, et al. Designed inhibitors of insulin-degrading enzyme regulate the catabolism and activity of insulin. *PLoS One*. 2010;5(5):e10504.